A&A 440, 391–402 (2005)
DOI: 10.1051/0004-6361:20042090

Astronomy & Astrophysics

A quantitative study of proton irradiation and UV photolysis of benzene in interstellar environments

R. Ruiterkamp[1], Z. Peeters[2], M. H. Moore[3], R. L. Hudson[4], and P. Ehrenfreund[2]

[1] Leiden Observatory, PO Box 9513, 2300 RA Leiden, The Netherlands
e-mail: ruiterka@strw.leidenuniv.nl
[2] Astrobiology Laboratory, Leiden Institute of Chemistry, PO Box 9502, 2300 RA Leiden, The Netherlands
[3] NASA/Goddard Space Flight Center, Code 691, Greenbelt, Maryland 20771, USA
[4] Department of Chemistry, Eckerd College, St. Petersburg, Florida 33733, USA

Received 29 September 2004 / Accepted 13 May 2005

Abstract. Benzene is an essential intermediate in the formation pathways of polycyclic aromatic hydrocarbons (PAHs) and carbon dust. Therefore, it is important to understand the interplay of formation and destruction in order to assess the lifetime of benzene in space. We performed UV photolysis and proton (0.8 MeV) bombardment experiments on benzene (C_6H_6) isolated in inert argon matrices and in oxygen-rich solid mixtures in the laboratory. The destruction of benzene in different chemical environments was measured for both methods of energetic processing. Additionally, we quantitatively determined the absorbed photon fraction in the sample layers when exposed to our UV lamp with actinometry. This enabled us to derive destruction cross sections for benzene for both UV photolysis and proton bombardment allowing us to compare these two ways of energetic processing. The laboratory data were extrapolated to different interstellar environments and we found that benzene is efficiently destroyed in diffuse interstellar clouds, but could survive dense cloud environments longer than the average lifetime of the cloud. Benzene is likely to survive in the dense parts of circumstellar envelopes around carbon-rich AGB stars but only in a very finite region where UV photons are attenuated.

Key words. ISM: molecules – ISM: abundances – ISM: clouds

1. Introduction

In the circumstellar envelopes of carbon-rich evolved stars a complex carbon chemistry occurs that is analogous to carbon soot formation in a candle flame or in industrial smoke stacks. Acetylene (C_2H_2) polymerization is assumed to be the starting point for the development of hexagonal aromatic rings of carbon atoms. These aromatic rings probably react further to form large aromatic networks (Frenklach & Feigelson 1989; Cherchneff et al. 1992). The most abundant complex organic molecules (not CO) in the gas phase are polycyclic aromatic molecules (PAHs). These compounds are likely responsible for the unidentified infrared emission bands (UIBs) between 3 and 17 μm (Hudgins & Allamandola 1999a,b; Tielens et al. 1999), a spectroscopic signature observed in our and external galaxies. PAH ions are also suggested as the carriers of the Diffuse Interstellar absorption Bands (DIBs) that are found in the ultraviolet (UV) and visual ranges of the spectrum toward sources that probe the diffuse interstellar medium (see Herbig 1995, for a review). Laboratory simulations in combination with interstellar observations support the idea that the predominant fraction of carbon not locked up in CO is incorporated into solid macromolecular carbon (e.g. Pendleton & Allamandola 2002) or amorphous and hydrogenated amorphous carbon (Pendleton & Allamandola 2002; Dartois et al. 2004).

Benzene is the key molecule in the formation pathways of those complex carbon compounds in space. Benzene detection has been claimed in the Infrared Space Observatory (ISO) spectrum of the circumstellar envelope around CRL 618 (Cernicharo et al. 2001). The observed absorption band was restricted to the part of the circumstellar envelope where densities are high and UV radiation from the star and the surrounding interstellar medium are attenuated. The models of Woods et al. (2002) indicate rapid destruction of molecules in the circumstellar envelope of CRL 618 at a distance of $\sim 10^{16}$ cm from the central star.

Ices can be found in a range of astronomical environments such as covering silicate and carbon dust surfaces in dense interstellar clouds, on comets and on planetary surfaces (see Ehrenfreund et al. 2003). Ices in the interstellar medium (ISM) are dominated by H_2O with contributions from CO, CO_2 and CH_3OH and traces of molecules such as CH_4 and NH_3 (Whittet et al. 1996; Gibb et al. 2004). The composition of interstellar ice is governed by dynamic processes such as accretion/sublimation, barrier-less chemical reactions and energetic processing by UV and cosmic ray particles. The interplay between these mechanisms determines the composition and abundance of molecular species in ice layers (Johnson 1996; Greenberg et al. 2000; Sandford et al. 2001; Roser et al. 2001).

Table 1. Observed wavenumbers and intrinsic strengths (A) for benzene infrared bands in argon matrices.

Band[a]	$\tilde{\nu}^a$ (cm^{-1})	$\tilde{\nu}^b$ (cm^{-1})	A^a (cm $molec^{-1}$)	Assignment[a,c]
ν_{20}, e_{1u}	3103	3095		CH a.s.
$\nu_1 + \nu_6 + \nu_8$, e_{1u}	3080	3075	1.1×10^{-17}	comb.
$\nu_8 + \nu_{19}$, e_{1u}	3048	3043		comb.
$\nu_{17} + \nu_5$, e_{1u}	1960	1957	–	comb.
$\nu_{17} + \nu_{10}$, e_{1u}	1808	1812	–	comb.
ν_{19}, e_{1u}	1481	1481	4.7×10^{-18}	CC a.s.
ν_{18}, e_{1u}	1038	1038	2.5×10^{-18}	CH i.p.b.
ν_{11}, a_{2u}	674	678	2.0×10^{-17}	CH o.p.b.

[a] Brown & Person (1978).
[b] This study.
[c] Strazzulla & Baratta (1991).
CH a.s. = CH aromatic stretching mode.
comb. = combination mode.
CC a.s. = CC aromatic stretching mode.
CH i.p.b. = CH in plane bending mode.
CH o.p.b. = CH out of plane bending mode.

Although not yet detected, benzene and PAHs could be present in dense molecular clouds where they are condensed into ice mantles on interstellar grains. UV photolysis and energetic proton bombardment experiments provide a means to determine the effects of different interstellar radiation environments. Matrix isolation spectroscopy in inert matrices is the most readily available technique to simulate gas phase behavior of interstellar molecules at diffuse and dense cloud temperatures. With this technique the stability of molecules under simulated interstellar conditions can be used as an upper limit for space conditions. Comparison of matrix isolation results to gas phase data shows a reasonable agreement (see Sect. 4, destruction in the interstellar gas may proceed at higher rates since intermolecular interactions are reduced). Previous studies of benzene in astronomical environments focussed on solid benzene layers that were bombarded with low energy (keV) helium ions (Strazzulla & Baratta 1991).

In this paper we describe laboratory studies of benzene in a low temperature Ar matrix and in oxygen-rich matrices (H_2O, CO and CO_2) under simulated interstellar conditions. The quantitative effects of UV photolysis and 0.8 MeV proton radiolysis on benzene in these solid matrices are compared. In Sect. 2 we briefly describe the laboratory set-ups and techniques used. In Sect. 3 we present the spectra and assignments of destruction fragments. In Sect. 4 the quantitative effects of UV photolysis and proton bombardment in binary solids are discussed and extrapolated in Sect. 5 for interstellar environments. We draw conclusions in Sect. 6.

2. Experimental

Two sets of experiments have been performed on each solid mixture in order to investigate the effects of proton irradiation and UV photolysis on benzene in Ar, H_2O, CO and CO_2 matrices. The proton irradiation experiments were performed at the NASA Goddard Space Flight Center while the UV photolysis experiments were performed at the Leiden Institute of Chemistry. The two experimental systems that were used are comparable. Both systems consist of a stainless steel high vacuum chamber with a suspended sample target that is attached to the cold end of a cryostat (∼14 K). The sample target can alternatively face a deposition system, an energy source (proton beam or hydrogen flow lamp) and a FTIR spectrometer.

The vapor of multiply distilled C_6H_6 or H_2O, and laboratory grade gases Ar, CO and CO_2 (Praxair 99.995%) were mixed in a gas manifold and deposited onto the cold sample target. Condensation was typically at a rate of 2 to 5 μm h^{-1}. The ratio of benzene to matrix constituent was between 1:350 and 1:700 for the matrix isolation experiments in Ar, 1:5 for the H_2O mixtures, 1:30 for the CO mixtures and 1:20 for the CO_2 mixtures. Argon isolated sample thicknesses in MeV bombardment experiments were typically ∼10 μm and the incident 0.8 MeV protons had a projected range of ∼20 μm (Northcliffe & Shilling 1970). Sample thicknesses in oxygen rich ices were typically 1 μm. Stopping powers (eV cm^2 g^{-1}) for 0.8 MeV protons in each experiment were calculated using the SRIM2003 software package by Biersack and Ziegler (Biersack & Haggmark 1980; Ziegler 1977). We obtained 170.2, 274.1, 245.7 and 241.1 MeV cm^2 g^{-1} for pure Ar, H_2O, CO and CO_2 solid matrices, respectively and 307.1 MeV cm^2 g^{-1} for pure solid C_6H_6. UV photolysis experiments were performed in matrices less than ∼0.1 μm thick for the oxygen rich matrices and 1 μm for matrix isolation experiments in Ar, and are considered optically thin for the radiation wavelengths used. Sample preparation techniques and irradiation procedures used in proton bombardment experiments are described in Hudson & Moore (1995); Moore & Hudson (1998) and Gerakines et al. (2000). UV irradiation experiments were performed at a system pressure of $\sim 5 \times 10^{-8}$ mbar while the proton irradiation experiments were performed at a system pressure of $\sim 1 \times 10^{-7}$ mbar.

Protons were accelerated with a Van de Graaf generator located at the Cosmic Ice Laboratory at NASA Goddard Space Flight Center that delivered protons with an energy of 0.8 MeV to the sample. To deliver high energy photons to the samples, a microwave-powered hydrogen flow lamp (Opthos Instruments, similar to the lamp in Gerakines et al. 2000) was mounted on the setup. The lamp flux at a forward/reflected power ratio of 100/6 was 1.1×10^{14} photons cm^{-2} s^{-1} for the oxygen rich matrices and 4.5×10^{14} photons cm^{-2} s^{-1} for the matrix isolation experiments in Ar. These values were derived from the conversion of O_2 to O_3 when irradiated with UV photons (actinometry). Details on this calibration method can be found in Cottin et al. (2003). The average photon energy over the entire lamp spectrum is calculated to be 7.41 ± 0.23 eV. The total flux of Ly_α emission is at most 5% of the total energy between 100 and 200 nm (Cottin et al. 2003).

In the proton bombardment experiments we used reflection infrared spectroscopy on an ice covered aluminium sample mirror suspended in a FTIR spectrometer (Mattson, spectral range 4000–400 cm^{-1} and resolution 4 cm^{-1}). In the UV photolysis

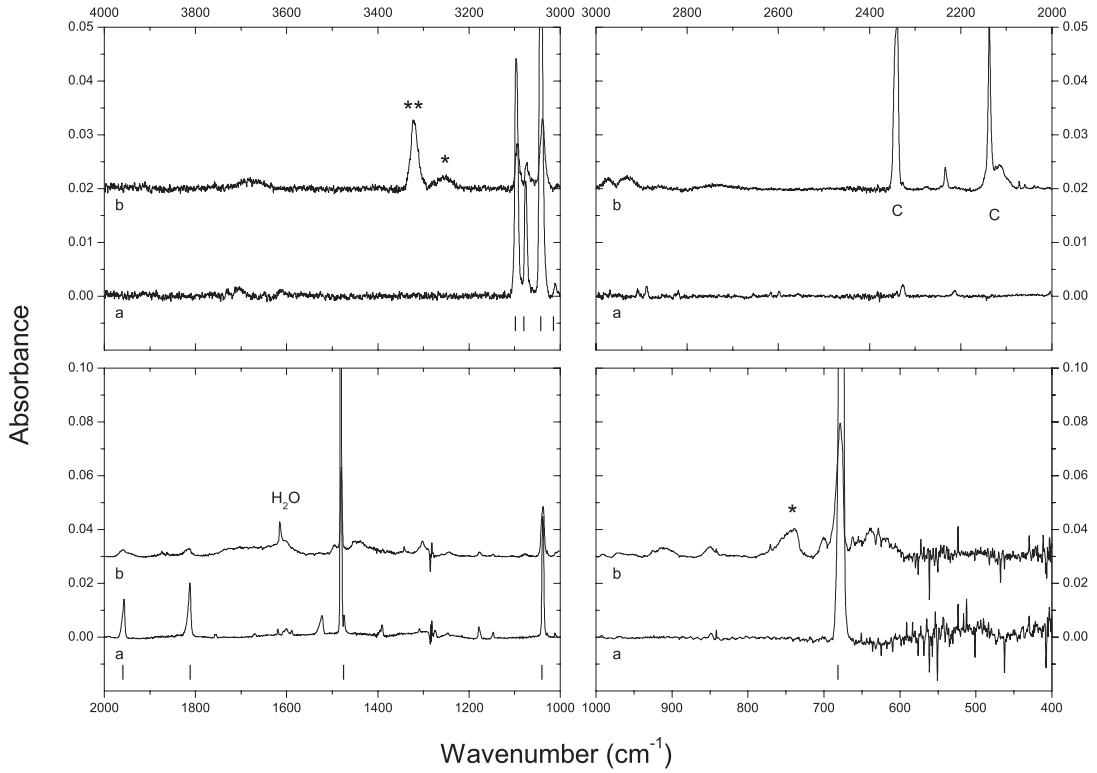

Fig. 1. IR spectrum of benzene isolated in argon (1:500) in the range 4000–2000 cm^{-1} (*top panels*) and 2000–400 cm^{-1} (*bottom panels*). Trace **a)** depicts the spectrum of C_6H_6/Ar before irradiation and trace **b)** shows the spectrum after proton bombardment to a total dose of ∼10 eV $molecule^{-1}$. Vertical dashes indicate the position of benzene spectral features. A single asterisk indicates a transition of acetylene and a double asterisk indicates matrix isolated methylacetylene. Contaminations from the vacuum chamber are indicated by a "C" (indicated are CO_2 and CO as contaminants after proton bombardment).

experiments we used transmission spectroscopy of a thin film of ice on a CsI sample window suspended in a Biorad FTIR spectrometer with spectral range 4000–400 cm^{-1} at resolution 1 cm^{-1} (Peeters et al. 2003).

3. Results

3.1. Proton bombardment and UV photolysis of solid C_6H_6

We exposed layers of pure solid benzene to 0.8 MeV protons and UV photolysis. Vibrational assignments before and after exposure were obtained using the work of Strazzulla & Baratta (1991) and references therein (see Table 1). Identical products were observed in proton bombardment and UV photolysis, although due to the thin sample layer in UV photolysis experiments not all products could be observed. Our results are used for quantitative analysis (see Sect. 4) and we refer to Strazzulla & Baratta (1991) for detailed spectra.

3.2. Proton bombardment and UV photolysis of C_6H_6 matrix isolated in Ar

A frozen layer of a C_6H_6/Ar mixture with a ratio of ∼1:500 was subjected to irradiation with high energy (0.8 MeV) protons and the destruction of the benzene molecule was monitored by infrared spectroscopy. For band identification, we compared our spectra to matrix isolated benzene spectra from Brown & Person (1978) and pure benzene spectra from Strazzulla & Baratta (1991). Most of the newly appearing bands could be identified although some bands appear slightly shifted between pure and isolated benzene, possibly due to matrix effects. Figure 1 shows the full mid-IR spectrum of benzene isolated in an argon matrix before and after proton irradiation. Figure 2 shows enlargements of two regions of spectra of proton irradiated benzene isolated in argon. Figure 2 also includes the spectrum of acetylene for comparison.

Table 2 lists the new bands (and their assignments) that appear after proton bombardment and UV photolysis of benzene isolated in an argon matrix, compared to literature values for 3 keV proton bombardment of frozen pure benzene layers. The features that appear at 2071 cm^{-1} in UV photolysis and 1904 cm^{-1} in proton bombardment experiments could not be assigned. Features at 2350 and 2140 cm^{-1}, peaks assigned to CO_2 and CO, respectively are a result of contaminants in the setup. CO_2 and CO form through reaction of H_2O dissociation products such as OH radicals with contaminants from the vacuum chamber. The long experiment run times (up to 11 h) explain the large quantities of CO and CO_2 observed.

3.2.1. The case of acetylene

Since benzene can be formed through the polymerization of three acetylene molecules, it is expected that decomposition of

Table 2. Observed new spectral bands after keV He^+ bombardment of pure benzene (Strazzulla & Baratta 1991, Col. A), MeV p^+/UV irradiation of pure benzene in this study (Col. B) and MeV p^+/UV processing of benzene isolated in argon matrices (Col. C). Note that the same destruction products appear when matrix isolated benzene is exposed to protons or UV (only the intensity of appearing bands differs according to the method of processing).

A pure C_6H_6 cm^{-1} (μm)	B pure C_6H_6 cm^{-1} (μm)	C isolated C_6H_6/Ar cm^{-1} (μm)	Assignment
–	–	3321 (3.01)	MIS HC_2CH_3
–	–	3302 (3.03)	MIS C_2H_2
3288 (3.04)	3278 (3.05)	–	C_2H_2 aggregates
3232 (3.09)	3232 (3.09)	3245 (3.08)	C_2H_2
2888 (3.46)	2888 (3.46)	2888 (3.46)	C-H aliph str
2824 (3.54)	2818 (3.55)	2820 (3.55)	C-H aliph str
2116 (4.73)	2107 (4.75)	2124 (4.71)	C≡C str monosubst C_2H_2
–	–	2071 (4.83)	?
1952 (5.12)	1956 (5.11)		subst C_6H_6
–	1904 (5.30)	–	?
1604 (6.23)	1604 (6.23)	–	C=C str subst C_6H_6
1556 (6.43)	1522 (6.57)	–	C=C str subst C_6H_6
1414 (7.07)	–	1391 (7.19)	comb band C_2H_2
1180 (8.47)	–	1180 (8.47)	C-H ip bend C_6H_6
1152 (9.76)	–	1146 (8.73)	C-H ip bend C_6H_6
1080 (9.26)	1075 (9.29)	1076 (9.29)	C-H ip bend C_6H_6
916 (10.92)	909 (11.00)	912 (10.97)	C-H op bend C_2H_2
770–730 (12.99–13.70)	770 (12.99)	–	C_6H_5?
754 (13.26)	758 13.19)	740 (1351)	C-H op bend C_2H_2
700 (14.29)	700 (14.29)	700 (14.29)	C-H op bend C_6H_6
648 (15.43)	631(15.85)	637 (15.70)	C-H op bend C_2H_2

MIS = matrix isolated. ip = in plane.
aliph = aliphatic. op = out of plane.
asymm = asymmetric. str = stretching vibration.
bend = bending vibration. subst = substituted.
comb = combination mode.

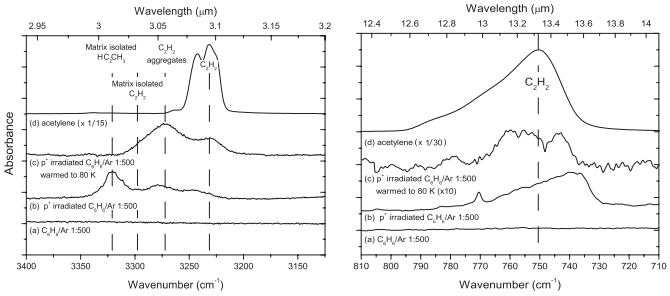

Fig. 2. Identification of acetylene infrared bands in the 3400–3100 cm^{-1} and 810–710 cm^{-1} range after proton bombardment of benzene isolated in argon (1:500). From bottom to top, traces show **a)** an unirradiated C_6H_6/Ar sample with a ratio of 1:500 at ~14 K, **b)** the same sample irradiated to a dose of ~10 eV $molecule^{-1}$, **c)** the same proton irradiated sample warmed to 80 K (to remove all argon) that shows the disappearance of the band at 3321 cm^{-1} and 3302 cm^{-1} attributed to matrix-isolated methylacetylene and acetylene, respectively, and **d)** unirradiated pure (not isolated) acetylene at ~14 K. Some spectra were scaled with the factor given in parentheses.

benzene yields acetylene. Nevertheless, we considered many other small molecules in our search for radiolytic and photolytic products. Among the investigated compounds were molecules, radicals and ions such as methane, ethane, propane, ethylene, phenyl radical, benzene ions and propylene.

Assignments by Strazzulla & Baratta (1991) were used to identify most of the new bands after energetic processing. However, some differences were found (see Table 2). The weak band at 3302 cm^{-1} could be assigned to matrix isolated acetylene by comparing to literature values (George et al. 2003). The band at 3321 cm^{-1} could be assigned to matrix isolated methylacetylene (Jacox & Milligan 1974, HC_2CH_3). Upon warm up of the irradiated sample to above the sublimation temperature of argon (~45 K) the isolated methylacetylene feature at 3321 cm^{-1} disappeared and the bands around 3278 cm^{-1} and 3245 cm^{-1} increased in intensity due to sublimation of the matrix. Strazzulla & Baratta (1991) assigned the band around 3278 cm^{-1} to monosubstituted acetylene. Since this band increases upon warm up to 80 K we think that this band can be tentatively assigned to C_2H_2 aggregates which could also include complexes between HC_2CH_3 and C_2H_2. However, these experiments were not specifically aimed to give a definitive assignment of the bands that appear after energetic processing and future work is needed to investigate these details.

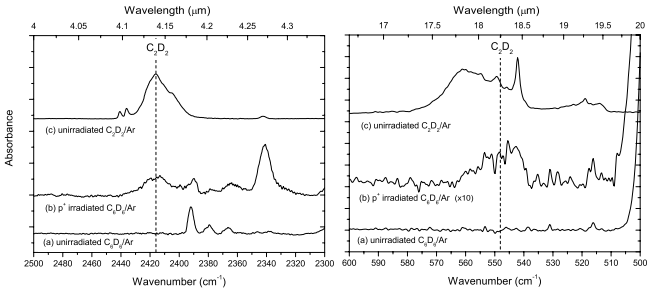

Fig. 3. IR spectra of a C_6D_6/Ar samples after proton bombardment between 2500–2300 and 600–500 cm^{-1}. Trace **a)** shows an unirradiated C_6D_6/Ar sample with a ratio of 1:500 at ∼14 K, **b)** the same sample, after irradiation with protons to a total dose of 10 eV molecule^{-1} and **c)** an unirradiated C_2D_2/Ar sample with a ratio of 1:100 at ∼14 K. The figure shows that upon proton bombardment of C_6D_6 new bands appear that can be assigned to C_2D_2, confirming the formation of acetylene by energetic processing of C_6H_6. CO_2 is observed at 2340 cm^{-1} as a radiolysis contaminant.

The right panel of Fig. 2 shows the spectral region including the ν_5 mode of acetylene between 730–770 cm^{-1}. Unfortunately transitions of dehydrogenated benzene (i.e. C_6H_5, C_6H_4, ...) fall in this region (Strazzulla & Baratta 1991) making a clear identification of C_2H_2 impossible. Therefore, we can not use this region to determine the column density of C_2H_2 in our experiments.

However, the production of acetylene can further be deduced from a comparison between the radiolysis products of matrix isolated C_6D_6 and matrix isolated C_2D_2. From Fig. 3 we see that the bands that appear at 2420 and 560 cm^{-1} in the proton bombardment experiments of a C_6D_6/Ar (1:500) sample (trace b), are well reproduced by a C_2D_2/Ar sample mixture (trace c). Figure 3 shows that upon proton bombardment of C_6D_6 new bands appear that can be assigned to C_2D_2 confirming the formation of acetylene from C_6H_6 destruction. No attempt is made to calculate formation cross sections for acetylene in these experiments.

3.3. Benzene in oxygen rich ices

3.3.1. Binary solids: C_6H_6/H_2O

In Fig. 4 we show the spectrum of a C_6H_6/H_2O mixture before and after proton bombardment. We compare the quantitative results for photolysis and radiolysis of C_6H_6/H_2O (1:5) samples in Sect. 4. After irradiation new bands appeared. Table 3 lists the wavenumber (cm^{-1}) and wavelength (μm) of the new bands as well as their possible assignment. During proton bombardment we found new bands around 763 and 746 cm^{-1} that were not seen after UV photolysis.

Due to the strong UV absorption of H_2O, only thin sample layers (<0.1 μm) could be used to allow full penetration of the UV through the sample. Therefore, in UV irradiated solid H_2O the photoproducts are produced at much smaller abundances than in proton bombarded solid H_2O. By comparing to literature values from Moore & Hudson (2000) we have assigned the weak band at 2870 cm^{-1} to H_2O_2. Samples were bombarded with a total dose of ∼25 eV molecule^{-1}.

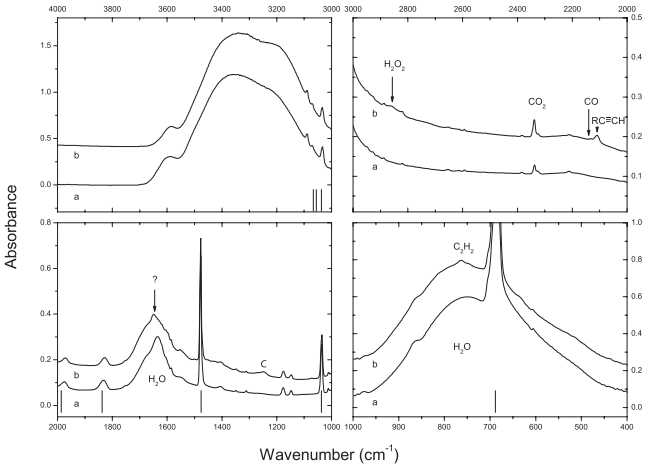

Fig. 4. New bands that appeared in solid C_6H_6/H_2O (1:5) after proton irradiation. Trace **a)** shows the spectrum before radiolysis and trace **b)** depicts the same spectral region after radiolysis to a dose of ∼25 eV molecule^{-1}. New bands are blended with the strong H_2O absorption bands and are not clearly visible. See Table 3. Benzene features are marked with vertical tick marks and contamination from the vacuum system is marked with "C".

Table 3. Observed new features after proton and UV irradiation of solid C_6H_6/H_2O (1:5) samples. Figure 4 shows the spectra of solid C_6H_6/H_2O before and after proton irradiation. Infrared modes of H_2O could obscure bands of some photoproducts. Additionally, due to the thin sample layers (<0.1 μm) UV irradiated samples show benzene photoproducts only at very small abundances.

Observed transition				Assignment
p^+		UV		
(cm^{-1})	(μm)	(cm^{-1})	(μm)	
2870	3.48			H_2O_2*
2340	4.27	2340	4.27	CO_2
2140	4.67	2140	4.67	CO
2110	4.53			C≡C str monosubst C_2H_2
1653	6.05			?
763	13.11			C_2H_2
746	13.40			C_2H_2

Also observed in UV photolysis of pure solid H_2O (Gerakines et al. 1996).

During UV photolysis of solid H_2O, molecules are dissociated to form H_2O_2, and H· and OH· radicals. During proton bombardment of water ice apart from H· and OH· radicals, OH^- and H_3O^+ ions could be formed. These irradiation products can subsequently react with other species in the matrix. Proton-irradiation of benzene in water ice could then yield such species as phenol (C_6H_5OH). However, we did not detect phenol. Production of CO_2 and CO features upon energetic processing in these matrices are due to the oxidation of benzene fragments.

3.4. Binary solids: C_6H_6/CO

Proton irradiation of solid C_6H_6/CO (1:30) samples resulted in the destruction of benzene and the formation of new bands (see

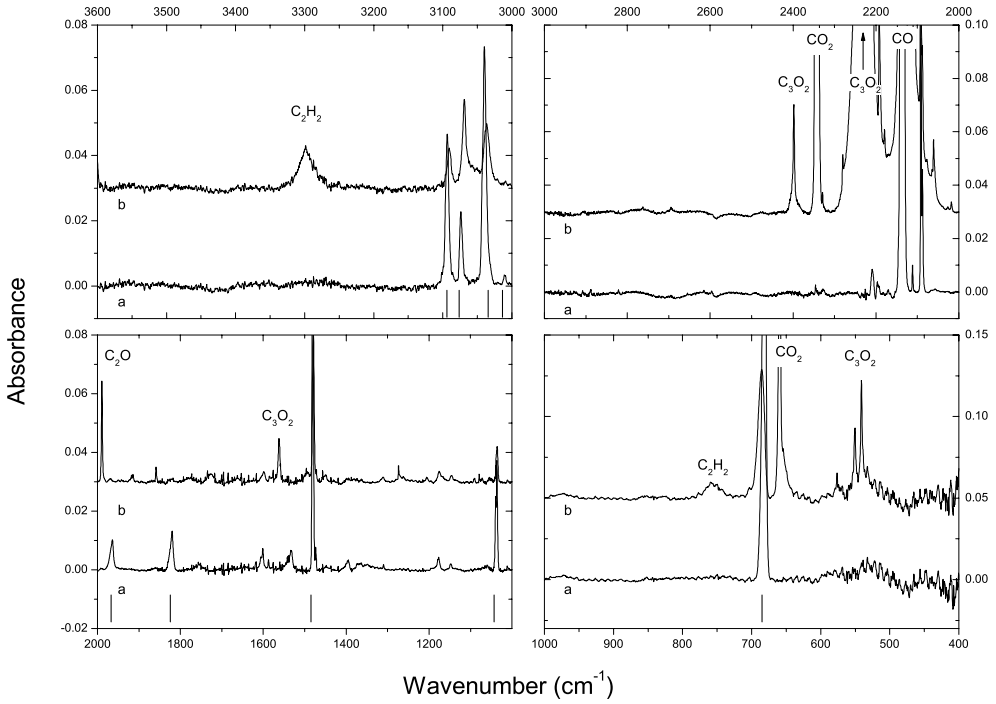

Fig. 5. The spectra of solid C_6H_6/CO (1:30) before and after proton irradiation. Trace **a)** depicts the spectral region before irradiation, while trace **b)** shows the spectrum after irradiation to a total dose of ∼15 eV molecule^{-1}. Bands and possible assignments are listed in Table 4. Benzene features are marked with vertical tick marks.

Fig. 5). The observed bands that appeared after energetic processing and their assignments are listed in Table 4. During proton irradiation new bands appeared that were not seen during UV photolysis. Apart from the bands due to CO_2, new bands appeared at 2398, 2242, 1562, 960, 550 and 541 cm^{-1}. We look at the quantitative difference between photolysis and radiolysis of C_6H_6/CO solids in Sect. 4.

Due to the high dissociation energy (11 eV) of CO no single-step photodestruction can occur during UV photolysis. However, formation of activated CO molecules can lead to subsequent chemical reactions and may yield a small amount of CO_2 during UV photolysis (Okabe 1978). We see a number of UV photoproduct bands that are not seen after proton irradiation and vice versa. Bands that appeared solely during UV photolysis are located at 1585, 1525, 832, 744 and 580 cm^{-1} and are assigned in Table 4. New products are primarily CO_2 and C_3O_2.

3.5. Binary solids: C_6H_6/CO_2

We exposed solid C_6H_6/CO_2 (1:20) samples to UV irradiation and proton bombardment. New features that appeared after irradiation of C_6H_6/CO_2 samples are given in Table 5 as well as possible assignments. Energetic processing of pure solid CO_2 yielded CO in both UV photolysis and radiolysis experiments. Figure 6 shows a comparison between the deposited sample before and after proton irradiation to a total dose of ∼15 eV molecule^{-1}. We look at the quantitative results of photolysis and radiolysis of C_6H_6/CO_2 samples in Sect. 4.

During proton bombardment of C_6H_6/CO_2 samples new bands appeared at 3298, 3252, 1880 and 763 cm^{-1} that have no counterpart in UV photolysis experiments. New bands around 3298 and 3252 cm^{-1} could possibly be assigned to acetylene in a CO_2 environment.

4. Discussion

In the quantitative analysis that is described in this section only low proton and photon fluences are used and we may assume optically thin sample layers in all experiments.

For calculation of the destruction cross section of benzene isolated in an Ar matrix we have used the broad C-H stretching vibration around 3103 cm^{-1}, the strong aromatic C=C stretching vibration at 1481 cm^{-1} and the C-H in plane bending vibration at 1038 cm^{-1}. All oxygen rich matrices (H_2O, CO_2 and CO) used show strong absorptions in the infrared and therefore not all infrared active benzene bands could be measured. This especially applies to the broad bands of water. We have used the 1481, 1040 and 688 cm^{-1} bands of benzene in all quantitative analyses when not obscured by absorption bands of the matrix material.

4.1. Energy dose delivered by photolysis and proton bombardment

4.1.1. Photolysis

The energy absorbed by a benzene molecule in our UV irradiation experiments can be expressed as a dose in units of [eV molecule^{-1}] by:

$$D_{\mathrm{UV}} = \frac{\langle E_{h\nu}\rangle \Phi_{\mathrm{abs}} t}{N_0}. \quad (1)$$

Table 4. Observed new features after proton and UV irradiation of solid C_6H_6/CO (1:30) samples. Figure 5 shows the spectra of solid C_6H_6/CO before and after proton irradiation. UV irradiation of CO does not photodissociate the CO molecule directly and fewer photoproduct bands appeared in these experiments compared to proton bombarded C_6H_6/CO.

Observed transition				Assignment
p^+		UV		
(cm^{-1})	(μm)	(cm^{-1})	(μm)	
3741	2.67			CO_2^*
3597	2.78			CO_2^*
3297	3.03			C_2H_2, substituted
3252	3.08			C_2H_2
2398	4.17			$C_3O_2^*$
2340	4.27	2340	4.27	CO_2^*
2242	4.46			$C_3O_2^*$
1989	5.03	1989	5.03	C_2O^*
1857	5.39	1857	5.39	HCO·
		1585	6.31	?
1562	6.40			$C_3O_2^*$
		1525	6.56	?
1090	9.17	1090	9.17	HCO·
960	10.42			?
		832	12.02	C_2H_4?
		790	12.66	?
759	13.18			C_2H_2
		744	13.44	C_2H_2
660				CO_2^*
		580	17.24	?
550	18.18			$C_3O_2^*$
541	18.48			$C_3O_2^*$

* Also observed in UV photolysis of pure CO. See Gerakines et al. (1996) and Trottier & Brooks (2004) and references therein.

Table 5. Observed new features after proton and UV irradiation of solid C_6H_6/CO_2 (1:20) samples. In Fig. 6 we show the spectra before and after proton bombardment. Features denoted with question marks are broad bands likely due to organic residues.

Observed transition				Assignment
p^+		UV		
(cm^{-1})	(μm)	(cm^{-1})	(μm)	
3298	3.03			substituted C_2H_2
3252	3.08			C_2H_2
2140	4.67	2140	4.67	CO^*
2090	4.79	2090	4.79	$^{13}CO^*$
2042	4.90	2042	4.90	CO_3^*
1880	5.32			CO_3^*
1723	5.80	1724	5.80	?
1692	5.91			?
1658	6.03			?
1300	7.69			?
1175	8.51			?
1072	9.33			?
1040	9.62	1040	9.62	O_3
974	10.27			?
797	12.55	798	12.53	
763	13.11			C_2H_2

* Also observed in UV photolysis of pure CO_2 and CO solids see Gerakines et al. (1996) and Trottier & Brooks (2004) and references therein.

Where $\langle E_{h\nu} \rangle$ is the average photon energy [eV photon^{-1}], $\Phi_{\rm abs}$ the absorbed photon flux [photons cm^{-2} s^{-1}], t is photolysis time [s] and N_0 is the column density of benzene at t = 0 [molecules cm^{-2}]. The determination of absorbed doses in UV experiments was previously described by Gerakines et al. (2000) where the authors used optically thick samples and assumed that all photons were absorbed in the sample. Here, we focus on optically thin samples that allow the use of first order reaction kinetics to describe the destruction of benzene. Therefore, we have performed simple actinometry experiments where a layer of solid O_2 is accreted onto the sample window before the deposition of a C_6H_6/Ar mixture. UV photons that enter the oxygen sample layer after passing through the C_6H_6/Ar layer can photolyze the O_2 molecules to form the infrared active O_3 with a strong band at 1040 cm^{-1}. By monitoring the conversion rate of the infrared inactive O_2 to the infrared active O_3 molecule during photolysis (see Cottin et al. 2003, for details) we can calculate the fraction of photons that is absorbed in the C_6H_6/Ar matrix. We assume a minimal effect on the results from interactions in the boundary layer. For the layer thicknesses used in these experiments argon does not absorb UV photons and thus all absorbed photons are absorbed by benzene.

We found that about 25% of the impinging photons were absorbed in a 1.25 μm layer of 1:500 solid C_6H_6/Ar mixture. Through the Beer law for spectroscopic absorption we can now calculate the UV absorption cross section for benzene isolated in argon and for pure benzene. The Beer law can be written as follows:

$$f_i = \frac{\Phi}{\Phi_0} = \mathrm{e}^{-\beta N_0} \quad (2)$$

where Φ_0 and Φ are the flux of the UV photons before and after passing through the C_6H_6/Ar sample [photons cm^{-2} s^{-1}]. The value of Φ_0 is known from separate lamp calibration experiments where the O_3 formation rate is determined from irradiation of only an O_2 sample layer on the substrate (Cottin et al. 2003) while Φ was obtained from the O_2 to O_3 conversion rate in experiments described above. The ratio of these two fluxes (the absorptance, f_i) is the fraction of UV photons that is absorbed by benzene in the argon layer. Here, we neglect that the column density is a function of photolysis time and assume it is a constant for the short irradiation timescales considered here. Now, β can be regarded as the UV absorption cross section [cm^2 molecule^{-1}] integrated over the bands in the lamp spectrum where O_2 photodissociates (see Okabe 1978). Thus, when β is known we can calculate the ratio of Φ/Φ_0 for a given column density of absorbing molecules. The total photon

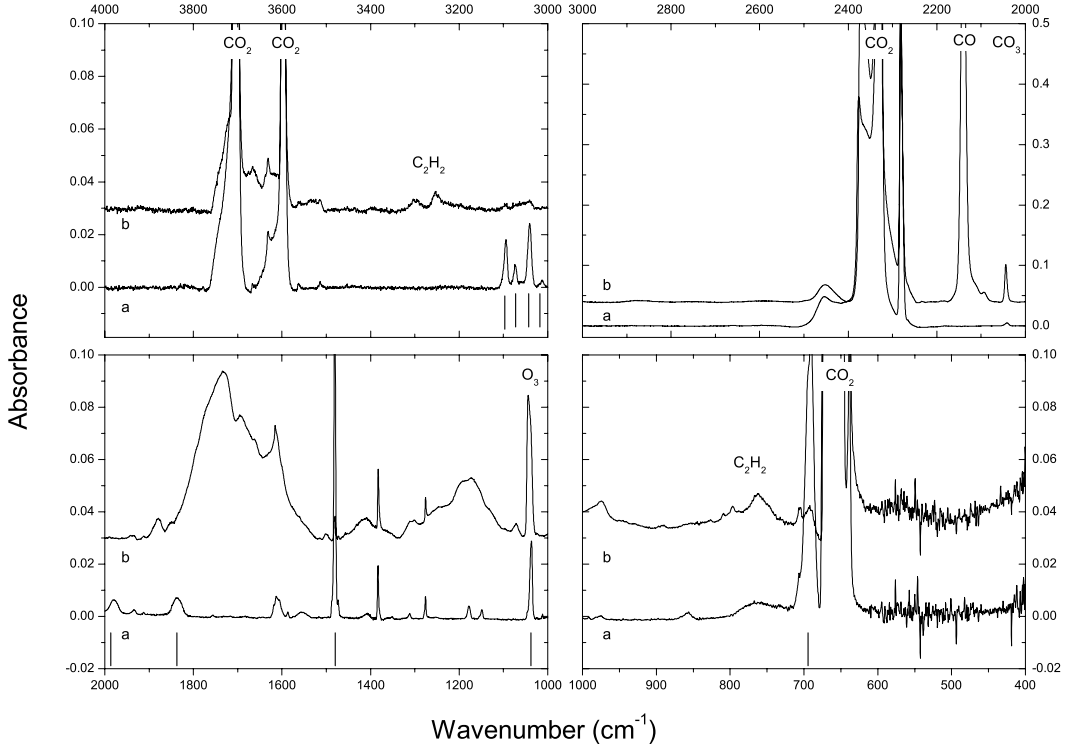

Fig. 6. New features that appeared in solid C_6H_6/CO_2 (1:20) after proton irradiation. Trace **a)** depicts the spectral region before irradiation, while trace **b)** shows the spectrum after irradiation to a total dose of ~15 eV molecule^{-1}. In Table 5 we list the band positions of photoproducts. Benzene features are marked with vertical tick marks. The broad bands that show after proton bombardment between 1800–1600 cm^{-1} and 1300–1100 cm^{-1} are possibly due to organic residues that may form from photoproducts.

flux that is absorbed by molecules in the sample (Φ_{abs}) can be expressed as:

$$\Phi_{abs} = (1 - f_i)\,\Phi_0. \quad (3)$$

For benzene isolated in argon we found $\beta = 3.2 \times 10^{-16}$ cm^2 molecule^{-1} and for pure benzene $\beta = 1.6 \times 10^{-17}$ cm^2 molecule^{-1}. Although not used in this work, similar experiments on layers of solid (not matrix isolated) H_2O, CO and CO_2 solids yielded $\beta = 4.5 \times 10^{-17}$, 1.8×10^{-18} and 1.1×10^{-18} cm^2 molecule^{-1} respectively.

4.1.2. Proton bombardment

Absorbed radiation energies per benzene molecule were calculated using the weighted average of the stopping powers for 0.8 MeV protons as described by Moore & Hudson (1998). The stopping power for 0.8 MeV protons in each experiment was calculated using the SRIM2003 software package by Biersack and Ziegler. For benzene we obtained a stopping power of 307.3 MeV cm^2 g^{-1}. For solid argon we obtained 170.2 MeV cm^2 g^{-1}. When a sample is bombarded with a proton beam with flux [p$^+$ cm^{-2} s^{-1}] for a time t [s] then the dose D [eV molecule^{-1}] is given by the product of the weighted average of the stopping powers per proton $\langle S_{av}\rangle$ [eV cm^2 g^{-1}], and the fluence divided by the average number of molecules per gram of sample.

$$D_{p^+} = \frac{\langle M_w\rangle\langle S_{av}\rangle\Phi_{p^+}t}{A_0} \quad (4)$$

where $\langle M_w\rangle$ [g mole^{-1}] is the weighted average of the molecular weights of all the molecules in the sample mixture, Φ_{p^+} the proton flux, t the irradiation time and A_0 Avogadro's constant [molecules mole^{-1}]. The obtained dose applies to a random molecule in the matrix with molecular mass $\langle M_w\rangle$. Generally, the dose absorbed by the different molecules in a mixture is weighted according to the electron fraction of each component. To obtain the dose absorbed per benzene molecule we substitute the average molecular weight in the sample ($\langle M_w\rangle$), with the molecular weight of benzene (m_w). The dose absorbed per benzene molecule in the matrix is now expressed in units of [eV molecule^{-1}]. Here we use the molecular weight of benzene instead of the relative electron abundance since this gives only small errors (much less than 1% for experiments with argon, and only in the order of 1% for all other experiments) and simplifies the calculation of the absorbed dose.

4.2. Destruction rate as a function of absorbed dose

For UV photolysis in an optically thin sample we assume first-order reaction kinetics to determine destruction cross sections. This is equivalent to writing $dN/dD = -kN$ where N is the sample's column density, D is the energy dose, and k is the rate constant. The destruction rate for photolysis of a molecule can be expressed using Eq. (1) as:

$$\frac{dN}{dt} = \frac{dN}{dD_{uv}}\frac{dD_{uv}}{dt} = \frac{dN}{dD_{uv}}\frac{E_{h\nu}\Phi_{abs}}{N_0} = -J_{uv}N \quad (5)$$

Table 6. Experimental parameters and destruction k and J values for pure benzene and benzene in different matrices. Numbers in parentheses indicate the exponential power, i.e. 1000 = 1.0(3).

Sample	$\langle S_{av} \rangle$	N_0	k		J	
	eV cm^2 g^{-1}	molecules cm^{-2}	molecule eV^{-1}		s^{-1}	
			p$^+$	UV	p$^+$	UV
pure C_6H_6	3.071(8)	1.5(16)	0.003	2.5(−4)	1.5(−5)	2.9(−6)
C_6H_6/Ar	1.725(8)	3.9(15)	0.107	0.006	2.9(−4)	3.7(−3)
C_6H_6/H_2O	2.830(8)	7.9(15)	0.011	0.011	5.0(−5)	1.3(−4)
C_6H_6/CO	2.391(8)	2.1(16)	0.109	0.024	4.2(−4)	2.7(−4)
C_6H_6/CO_2	2.441(8)	6.5(15)	0.147	0.039	5.7(−4)	4.8(−4)

with N the column density, $J_{uv} = \int_\lambda \sigma_\lambda \Phi_\lambda d\lambda = \sigma_{uv}\Phi_0$ [s^{-1}], with σ_{uv} the integrated UV destruction cross section [cm^2 molecule^{-1}] of the molecule over the lamp spectrum, and Φ_0 the integrated UV photon flux (see Cottin et al. 2003, for a detailed discussion on photolysis kinetics). When k_{uv} is defined as the negative slope in the graph of $\ln(N/N_0)$ against photolysis dose D_{uv} we obtain:

$$J_{uv} = \frac{k_{uv} E_{h\nu} \Phi_{abs}}{N_0}. \quad (6)$$

Also since $J = \sigma_{uv}\Phi_0$ with Φ_0 the integrated photon flux we can calculate σ_{uv}, the UV cross sections for destruction. Similarly, when we assume first order reaction kinetics for the proton bombardment experiments we obtain:

$$\frac{dN}{dt} = \frac{dN}{dD_{p^+}} \frac{dD_{p^+}}{dt} = \frac{dN}{dD_{p^+}} \frac{m_w \langle S_{av} \rangle \Phi_{p^+}}{A_0} = -J_{p^+} N. \quad (7)$$

Now when k_{p^+} is defined as the negative slope in the graph of $\ln(N/N_0)$ against proton radiation dose D_{p^+} we obtain:

$$J_{p^+} = \frac{k_{p^+} m_w \langle S_{av} \rangle \Phi_{p^+}}{A_0} = \sigma_{p^+} \Phi_{p^+}. \quad (8)$$

Half-lives [s] are defined as:

$$t_{1/2} = \frac{\ln 2}{J_{uv}}, \frac{\ln 2}{J_{p^+}}. \quad (9)$$

For our UV lamp we found that during the matrix isolation experiments the flux was $\Phi_0 = 4.5 \times 10^{14}$ photons cm^{-2} s^{-1} while during the oxygen rich matrix experiments the flux was reduced to $\Phi_0 = 1.1 \times 10^{14}$ photons cm^{-2} s^{-1}. The proton flux was constant at 1.2×10^{11} protons cm^{-2} s^{-1}.

The proton and UV destruction rates of benzene isolated in argon and pure benzene are shown in Fig. 7. Destruction rates for benzene in H_2O, CO and CO_2 are shown in Fig. 8. The obtained k and J values and the cross sections and half lifes are given in Tables 6 and 7. We find that the k values for UV experiments are less than those for proton bombardment experiments, except for the H_2O experiments. This difference may be due to the changes in optical properties of the ices that accompany photolysis, but not radiolysis (Baratta et al. 2002).

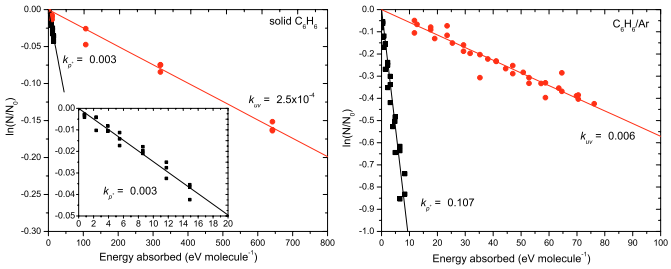

Fig. 7. Destruction of solid benzene (*left panel*) and benzene isolated in Ar (*right panel*) as a function of absorbed energy dose (• = UV, ■ = protons). The negative slope (k) of the plot is related to destruction cross section and half-life through Eqs. (7)-(9).

Table 7. Laboratory measured benzene destruction cross sections and half-lives for astronomically relevant ice mixtures. Numbers in parentheses indicate the exponential power, i.e. 1000 = 1.0(3).

Sample	σ		$t_{1/2}$	
	cm^2		s	
	p$^+$	UV	p$^+$	UV
pure C_6H_6	1.19(−16)	2.64(−20)	4.72(4)	2.4(5)
C_6H_6/Ar	2.39(−15)	8.13(−18)	2.36(3)	1.9(2)
C_6H_6/H_2O	4.03(−16)	1.23(−18)	1.40(4)	5.1(3)
C_6H_6/CO	3.38(−15)	2.42(−18)	1.67(3)	2.6(3)
C_6H_6/CO_2	4.65(−15)	4.39(−18)	1.21(3)	1.4(3)

5. Astrophysical implications

Destruction of benzene by proton bombardment in cold argon matrices is in the same range as for benzene locked up in CO or CO_2 samples but some 20 times faster than for proton bombardment of solid benzene and 6 times faster for benzene in H_2O.

Cold, matrix isolated benzene is destroyed some 1300 times faster by UV photons than solid benzene. UV destruction of benzene in CO_2 is slightly faster than for benzene in H_2O or CO ices but some 7 times slower than benzene isolated in an Ar matrix.

When we compare the effectiveness for destruction between each processing method we focus on the destruction

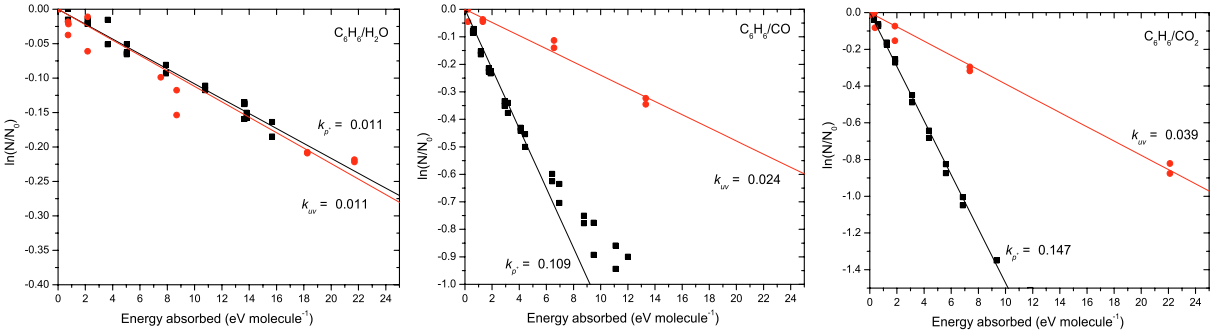

Fig. 8. Destruction of benzene in: water ice (1:5, *left panel*), in CO (1:30, *middle panel*) and in CO_2 (1:20, *right panel*) ices as a function of absorbed energy dose (• = UV, ■ = protons). The negative slope (k) of the plot is related to destruction cross section and half-life through Eqs. (7)-(9).

cross sections and find that proton bombardment of solid benzene is 4500 times more efficient than the UV photolysis of solid benzene. For matrix isolated benzene in argon we find that the destruction cross section of benzene by proton bombardment is some 300 times higher than for UV photolysis. Benzene locked up in solid CO or CO_2 is destroyed some 1000 times more efficiently by proton bombardment while benzene locked up in H_2O ice is destroyed 400 times more efficiently by proton bombardment. Apparently, the energy transfer in proton bombardment experiments is much more efficient which results in a higher benzene destruction rate.

Previous photolysis studies by Yokoyama et al. (1990) found a destruction cross section for gas phase benzene in the order of 1–5 $\times$ 10^{-17} cm^2. Those experiments were not measured in an astrophysical context (low temperatures and VUV). Our experiments are aimed at simulating interstellar conditions with low temperatures. Consequently, an inert, low perturbing argon matrix was used. As we will show in this section we find destruction cross sections 1.5–7 times lower in argon matrices. Perturbations that are expected from the matrix, such as dissipation of the delivered energy, may be responsible for differences compared to gas phase data and therefore, our matrix isolation experiments provide a lower limit for benzene destruction in interstellar environments. However, we shall use the destruction cross section derived from matrix isolated benzene experiments to extrapolate to gas phase benzene in interstellar environments. When hereafter gas phase benzene is mentioned, it refers to the destruction cross section of matrix isolated benzene.

We can now deduce half-lives for the benzene molecule in astronomical environments. Assuming first-order behavior over the entire range of photolytic and protolytic decay, we can define the astronomical half-life as:

$$t^*_{1/2} = \frac{\ln 2}{\Phi^* \sigma} \qquad (10)$$

where σ is the laboratory destruction cross section and Φ^* the interstellar UV photon or proton flux.

For the destruction rate of benzene in cold dense molecular clouds we use a UV flux of 10^3 photons cm^{-2} s^{-1} (Prasad & Tarafdar 1983) and a proton flux of 1 proton cm^{-2} s^{-1} > 1 MeV. The destruction rate of benzene in diffuse interstellar clouds is based on a UV flux of 10^8 photons cm^{-2} s^{-1} (Mathis et al. 1983)

Table 8. Interstellar half-lives [year] for benzene. No ices are expected in diffuse clouds and values were not calculated.

	$t_{1/2}$ p$^+$ year		$t_{1/2}$ UV year	
	dense	diffuse	dense	diffuse
pure C_6H_6	1.8(8)	1.8(7)	8.3(8)	8.3(3)
C_6H_6/Ar	9.2(6)	9.2(5)	2.7(6)	2.7(1)
C_6H_6/H_2O	5.5(7)	–	1.8(7)	–
C_6H_6/CO	6.5(6)	–	9.1(6)	–
C_6H_6/CO_2	4.7(6)	–	5.0(6)	–

and a galactic cosmic ray flux of 10 protons cm^{-2} s^{-1} > 1 MeV (Moore et al. 2001). In the solar system at 1 AU the photon flux from the sun (>6 eV) is 3.0 $\times$ 10^{13} photons cm^{-2} s^{-1} while the proton flux is dominated by solar flares that generate an average flux of 10^{10} protons cm^{-2} per year.

Figure 9 shows a summary of our results for all radiation environments. The figure shows the half-life (in years) as a function of the proton and photon flux. Different astronomical environments are indicated in the figure.

In Table 8 we give the half-life for benzene in diffuse and dense clouds. The half-life of benzene 3 $\times$ 10^6 years. This is longer than the estimated average lifetime for dense clouds (Elmegreen 2000). Based on the experiments on solid C_6H_6 the half-life for a solid layer of benzene that is exposed to the dense cloud UV field is ~8 $\times$ 10^8 years while the half-life for a solid benzene layer due to proton bombardment is ~2 $\times$ 10^8 years. This is well above the average lifetime of a dense molecular cloud. Destruction time scales of proton bombardment and UV photolysis of benzene in dense clouds are in the same range and we expect benzene to survive dense cloud environments.

As soon as the photon flux increases, such as in diffuse cloud environments, we find that benzene may only survive when sufficiently shielded against UV. The half-life of gas phase benzene due to UV photolysis in diffuse clouds is 27 years, as derived from the matrix isolated C_6H_6/Ar experiments. The proton flux in diffuse interstellar clouds is sufficient to destroy 50% of gas phase benzene in ~9 $\times$ 10^5 years. For solid benzene the high energy proton flux is only sufficient

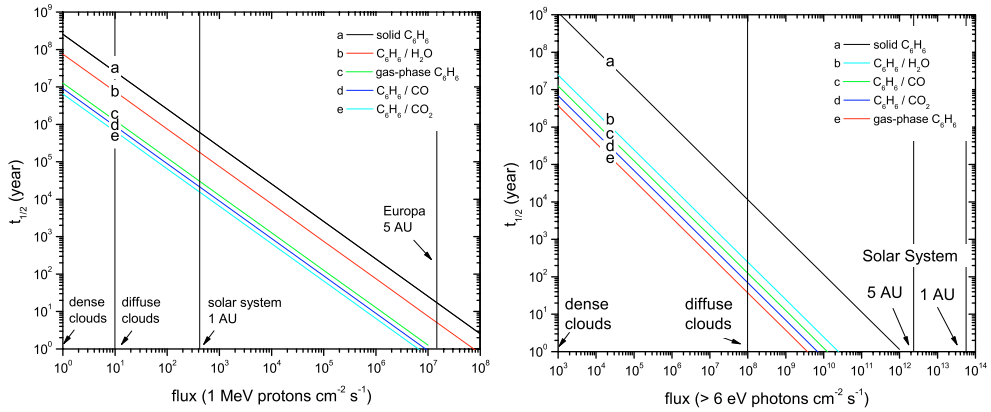

Fig. 9. Interstellar half-lives (see Eq. (10)) derived from laboratory C_6H_6/Ar and solid pure benzene experiments and for benzene embedded in solid H_2O, CO and CO_2 as a function of interstellar proton and photon flux. Half-lives in the left panel are given for proton fluxes and in the right panel for photon fluxes.

to destroy 50% of solid benzene in $\sim 2 \times 10^7$ years. Due to the low gas density in diffuse interstellar clouds, no ice layers are expected to cover the dust (Greenberg 1971; Mathis et al. 1983). The UV flux in diffuse interstellar clouds is 10^8 photons cm^{-2} s^{-1} (Mathis et al. 1983) and if we assume that icy grains at the boundary layers to dense clouds exist, typical time scales for the destruction of 50% of the initial column density are in the order of 100 years for photolysis of benzene in solid H_2O, CO and CO_2, while in the order of 1×10^6 years for radiolysis. Even if benzene is locked up in a solid, time scales for destruction by UV photons are much shorter than the life time of such layers in more diffuse media. We conclude that benzene cannot survive the conditions in the diffuse interstellar medium.

In the solar system at 1 AU from the sun, benzene exposed to the solar UV field has a half-life of $\sim 3 \times 10^3$ s and solid benzene $\sim 9 \times 10^5$ s. When we scale the solar UV flux at 1 AU to the vicinity of Jupiter (5 AU) we find a flux of 1.2×10^{12} photons cm^{-2} s^{-1} and can estimate residence times for benzene on icy moons. Destruction time scale for UV photolysis of benzene in water ice now becomes $\sim 5 \times 10^5$ s and for gas phase benzene $\sim 7 \times 10^4$ s. The 0.8 MeV magnetospheric proton flux at Europa has been estimated by Cooper et al. (2001) who obtained a proton flux of 1.5×10^7 protons cm^{-2} s^{-1}. The destruction time scale of benzene locked up in H_2O ice due to protons on Europa becomes in the order of 4 years and 0.6 years for gas phase benzene. If these fluxes are realistic and if any benzene is delivered to the surface of Europa by comets or volcanism, ions and photons would rapidly destroy it.

6. Conclusions

We have measured the stability of solid, matrix isolated and ice-embedded benzene against proton bombardment and UV photons. From our matrix isolation experiments we conclude that benzene is about 300 times more efficiently destroyed by proton bombardment than by UV photolysis per absorbed proton or photon. This indicates a more efficient energy transfer during radiolysis. Destruction of benzene leads to fragments of dehydrogenated benzene, methylacetylene and acetylene (and acetylene aggregates) that can be monitored by infrared spectroscopy.

Benzene is likely to survive in the dense parts of circumstellar envelopes but only in a very finite region where UV photons are attenuated. In the diffuse interstellar medium gas phase benzene has a very short half-life of 27 years. Therefore, in order to survive the diffuse interstellar medium conditions, benzene has to be converted into PAH molecules which are more stable against the harsh environment of high UV flux. In dense interstellar clouds benzene could survive in the gas phase or embedded in interstellar grain mantles for a period comparable to the lifetime of the cloud. In the solar system benzene will be rapidly destroyed even when embedded in the icy surface of outer solar system objects.

We conclude that benzene could be available for aromatic chemistry when sufficiently shielded in circumstellar envelopes from protons and UV photons and in dense clouds on the surface of interstellar icy grains.

Acknowledgements. We would like to thank the anonymous referees for their critical reading of the paper and for their suggestions to describe the results in identical units that allow a straightforward comparison that further supported our conclusions. This research was performed under SRON program MG-049, NWO-VI 016.023.003 and supported by NASA's SARA and Planetary Atmospheres Programs. The authors thank T. Millar for discussion.

References

Baratta, G. A., Leto, G., & Palumbo, M. E. 2002, A&A, 384, 343
Biersack, J. P., & Haggmark, L. 1980, Nucl. Instr. Meth. Phys. Res., 174, 257
Brown, K. G., & Person, W. B. 1978, Spectrochim. Acta, 34, 15
Cernicharo, J., Heras, A. M., Tielens, A. G. G. M., et al. 2001, ApJ, 546, L123
Cherchneff, I., Barker, J. R., & Tielens, A. G. G. M. 1992, ApJ, 401, 269

Cooper, J. F., Johnson, R. E., Mauk, B. H., Garrett, H. B., & Gehrels, N. 2001, Icarus, 149, 133
Cottin, H., Moore, M. H., & Bénilan, Y. 2003, ApJ, 590, 874
Dartois, E., Muñoz Caro, G. M., Deboffle, D., & d'Hendecourt, L. 2004, A&A, 423, L33
Ehrenfreund, P., Fraser, H. J., Blum, J., et al. 2003, PlanSS, 51, 473
Elmegreen, B. G. 2000, ApJ, 530, 277
Frenklach, M., & Feigelson, E. D. 1989, ApJ, 341, 372
George, L., Sanchez-Garćia, E., & Sander, W. 2003, J. Phys. Chem. A, 107, 6850
Gerakines, P. A., Moore, M. H., & Hudson, R. L. 2000, A&A, 357, 793
Gerakines, P. A., Schutte, W. A., & Ehrenfreund, P. 1996, A&A, 312, 289
Gibb, E. L., Whittet, D. C. B., Boogert, A. C. A., & Tielens, A. G. G. M. 2004, ApJS, 151, 35
Greenberg, J. M. 1971, A&A, 12, 240
Greenberg, J. M., Gillette, J. S., Muñoz Caro, G. M., et al. 2000, ApJ, 531, L71
Herbig, G. H. 1995, ARA&A, 33, 1974
Hudgins, D. M., & Allamandola, L. J. 1999a, ApJ, 516, L41
Hudgins, D. M., & Allamandola, L. J. 1999b, ApJ, 513, L69
Hudson, R. L., & Moore, M. H. 1995, Rad. Phys. Chem., 45, 779
Jacox, M. E., & Milligan, D. E. 1974, Chem. Phys., 4, 45
Johnson, R. E. 1996, BAAS, 28, 1072
Mathis, J. S., Mezger, P. G., & Panagia, N. 1983, A&A, 128, 212
Moore, M. H., & Hudson, R. L. 1998, Icarus, 135, 518
Moore, M. H., & Hudson, R. L. 2000, Icarus, 145, 282
Moore, M. H., Hudson, R. L., & Gerakines, P. A. 2001, Spectrochim. Acta, 57, 843
Northcliffe, L. C., & Shilling, R. F. 1970, Nucl. Data Tables, 7, 233
Okabe, H. 1978, Photochemistry of small molecules, A Wiley-Interscience Publication (New York: Wiley)
Peeters, Z., Botta, O., Charnley, S. B., Ruiterkamp, R., & Ehrenfreund, P. 2003, ApJ, 593, L129
Pendleton, Y. J., & Allamandola, L. J. 2002, ApJS, 138, 75
Prasad, S. S., & Tarafdar, S. P. 1983, ApJ, 267, 603
Roser, J. E., Vidali, G., Manicò, G., & Pirronello, V. 2001, ApJ, 555, L61
Sandford, S. A., Bernstein, M. P., Allamandola, L. J., Goorvitch, D., & Teixeira, T. C. V. S. 2001, ApJ, 548, 836
Strazzulla, G., & Baratta, G. A. 1991, A&A, 241, 310
Tielens, A. G. G. M., Hony, S., van Kerckhoven, C., & Peeters, E. 1999, in ESA SP-427: The Universe as Seen by ISO, 767
Trottier, A., & Brooks, R. L. 2004, ApJ, 612, 1214
Whittet, D. C. B., Schutte, W. A., Tielens, A. G. G. M., et al. 1996, A&A, 315, L357
Woods, P. M., Millar, T. J., Zijlstra, A. A., & Herbst, E. 2002, ApJ, 574, L167
Yokoyama, A., Zhao, X., Hintsa, E. J., Continetti, R. E., & Lee, Y. T. 1990, J. Chem. Phys., 92, 4222
Ziegler, J. F. 1977, The Stopping and Range of Ions in Matter: Vols. 2–6 (Pergamon Press)